Medicinal Inorganic Chemistry

How to cite: *Angew. Chem. Int. Ed.* **2023,** *62,* e202301074
International Edition: doi.org/10.1002/anie.202301074
German Edition: doi.org/10.1002/ange.202301074

# Reduction of Platinum(IV) Prodrug Hemoglobin Nanoparticles with Deeply Penetrating Ultrasound Radiation for Tumor-Targeted Therapeutically Enhanced Anticancer Therapy

*Ganghao Liang, Tumpa Sadhukhan, Samya Banerjee, Dongsheng Tang, Hanchen Zhang, Minhui Cui, Nicolás Montesdeoca, Johannes Karges,* and Haihua Xiao**

**Abstract:** The development of $Pt^{IV}$ prodrugs that are reduced into the therapeutically active $Pt^{II}$ species within the tumor microenvironment has received much research interest. In order to provide spatial and temporal control over the treatment, there is a high demand for the development of compounds that could be selectively activated upon irradiation. Despite recent progress, the majority of $Pt^{IV}$ complexes are excited with ultraviolet or blue light, limiting the use of such compounds to superficial application. To overcome this limitation, herein, the first example of $Pt^{IV}$ prodrug nanoparticles that could be reduced with deeply penetrating ultrasound radiation is reported, enabling the treatment of deep-seated or large tumors. The nanoparticles were found to selectively accumulate inside a mouse colon carcinoma tumor upon intravenous injection and were able to eradicate the tumor upon exposure to ultrasound radiation.

## Introduction

The $Pt^{II}$ complexes cisplatin, oxaliplatin, and carboplatin are some of the most frequently applied anticancer agents.[1] Recent statistical findings have suggested that these compounds are used in more than 50 % of all chemotherapeutic treatments worldwide.[2] Despite their undoubtful clinical success, the application of these metal complexes is hindered by their severe side effects (i.e., nausea, vomiting, kidney damage, and bone marrow suppression), poor tumor accumulation, and drug resistance.[3] To overcome these limitations, many research efforts have been invested over the last decades in the development of $Pt^{IV}$ complex prodrugs. Ideally, these compounds should remain stable and therefore inactive within healthy tissue, but be quickly reduced into the therapeutically active analogous compound within the cancerous tissue.[4] Previous studies have suggested that the reduction of the prodrug could be chemically mediated by intracellular reducing agents (i.e., glutathione, ascorbic acid, metallothionein, thioredoxin) which are present in high concentrations in cancerous cells.[5] However, as these reducing agents are also present in healthy cells, this activation mechanism is associated with poor spatial and temporal control as well as low reduction efficiency.[6] Studies have suggested that the reduction of the $Pt^{IV}$ prodrug could also be mediated by exposure of the compounds to light irradiation. The vast majority of reported $Pt^{IV}$ complexes are excited with ultraviolet ($\approx$365 nm) or blue ($\approx$450 nm) light.[7] Recent research studies have reported on the axial functionalization of the $Pt^{IV}$ center with a tetrapyrrolic photosensitizer that has an absorption in the red region (650 nm)[8] or with an aggregation-induced emission dye that could be excited in the near-infrared region (808 nm).[9] Despite these promising developments and impressive preliminary biological findings, these wavelengths are poorly penetrating the tissue (< 1 cm) and therefore could only find application for superficial applications. To enable the treatment of deep-seated or large tumors, there is an urgent need for the development

[*] G. Liang, D. Tang, H. Zhang, M. Cui, Prof. Dr. H. Xiao
Beijing National Laboratory for Molecular Sciences, Laboratory of Polymer Physics and Chemistry, Institute of Chemistry, Chinese Academy of Sciences
Beijing, 100190 (China)
and
University of Chinese Academy of Sciences
Beijing, 100049 (China)
E-mail: hhxiao@iccas.ac.cn
Dr. T. Sadhukhan
Department of Chemistry, SRM Institute of Science and Technology
Kattankulathur, Tamil Nadu 603203 (India)
Dr. S. Banerjee
Department of Chemistry, Indian Institute of Technology (BHU)
Varanasi, Uttar Pradesh 221005 (India)
N. Montesdeoca, Dr. J. Karges
Faculty of Chemistry and Biochemistry, Ruhr-University Bochum
Universitätsstrasse 150, 44780 Bochum (Germany)
E-mail: johannes.karges@ruhr-uni-bochum.de
Homepage: www.kargesgroup.ruhr-uni-bochum.de

of new methods for the activation of the $Pt^{IV}$ complexes with good spatiotemporal control.[10]

To circumvent this limitation, herein, the first example of a $Pt^{IV}$ complex that could be reduced upon exposure to ultrasound radiation for the treatment of deep-seated tumors is reported. Clinical studies have indicated that ultrasound radiation has more than an order of magnitude deeper tissue penetration than near-infrared light, allowing potentially for the treatment of deep-seated or large tumors. In addition, ultrasound treatments are generally suggested to be less invasive, easier to use, and clinics are typically already equipped with the necessary equipment.[11] Within this study, the frequently employed $Pt^{II}$ anticancer drug cisplatin was axially functionalized with aliphatic chains to form the $Pt^{IV}$ prodrug **Pt1**. Using density functional theory (DFT) calculations, the reduction of the $Pt^{IV}$ prodrug with ultrasound radiation using the tetrapyrrolic sonosensitizer was suggested. While remaining stable under physiological conditions, the metal complex was reduced in the presence of the sonosensitizer and exposure to ultrasound radiation. Based on the high lipophilicity of the metal complex, this compound was encapsulated with the biocompatible sonosensitizer **Hemoglobin** (**HGB**) into nanoparticles (**NP$^s$**). The nanoparticles were found to selectively accumulate inside a mouse colon carcinoma tumor upon intravenous injection. To highlight the ability of this medicinal technique for the treatment of very large or deep-seated tumors, the tumor tissue was covered with an additional 2 cm wide piece of chicken breast as a barrier. Upon exposure to ultrasound radiation, the $Pt^{IV}$ prodrug was activated at the tumor site, resulting in the release of cytotoxic cisplatin and almost complete eradication of the tumor (Scheme 1). These findings could pave the way towards the development of novel techniques and agents for the treatment of very large or deep-seated tumors.

## Results and Discussion

Previous studies have indicated that the axial coordination of a metal complex with a photosensitizer is able to mediate the reduction of the $Pt^{IV}$ center to $Pt^{II}$ through electron transfer from the excited photosensitizer to the metal core.[8,9] Over the last decades, much interest has been devoted sonosensitizers that can be excited with deeply penetrating ultrasound radiation for photoacoutic imaging.[12] Based on these findings, herein, the ability of the metal center to be reduced upon ultrasound radiation in the presence of a sonosensitizer was hypothesized. To avoid interference of light or radiation-absorbing moieties, the $Pt^{II}$ drug cisplatin (*cis*-diamminedichloridoplatinum(II)), which does not have any chromophoric ligands, was axially functionalized with aliphatic chains and the $Pt^{IV}$ prodrug **Pt1** formed. To study this hypothesis and evaluate which sonosensitizers could be suitable for the energy transfer, theoretical calculations were performed.

Using time-dependent DFT calculations, the possible reduction of the $Pt^{IV}$ prodrug was investigated. Based on the high biocompatibility and facile accessibility, the application of **HGB** as a suitable sonosensitizer was proposed. As the smallest molecular sonosensitizer unit of **HGB**, the heme group was used during the theoretical calculations. Due to the lability of oxygen from the axial position of the heme group, the penta- and hexa-coordinated heme group was considered. The calculations have indicated that the reduction from the penta-coordinated heme sonosensitizer is energetically unfavored (Figure S1). The following mechanism is proposed (Figure 1, figures of the optimized geometries of the compounds: Figure S2): Upon exposure to ultrasound radiation, the sonosensitizer is excited to an excited singlet state, requiring 28.1 kcal mol$^{-1}$. Through an intersystem crossing process, the spin of the excited electron is reversed and an excited triplet state is populated. While

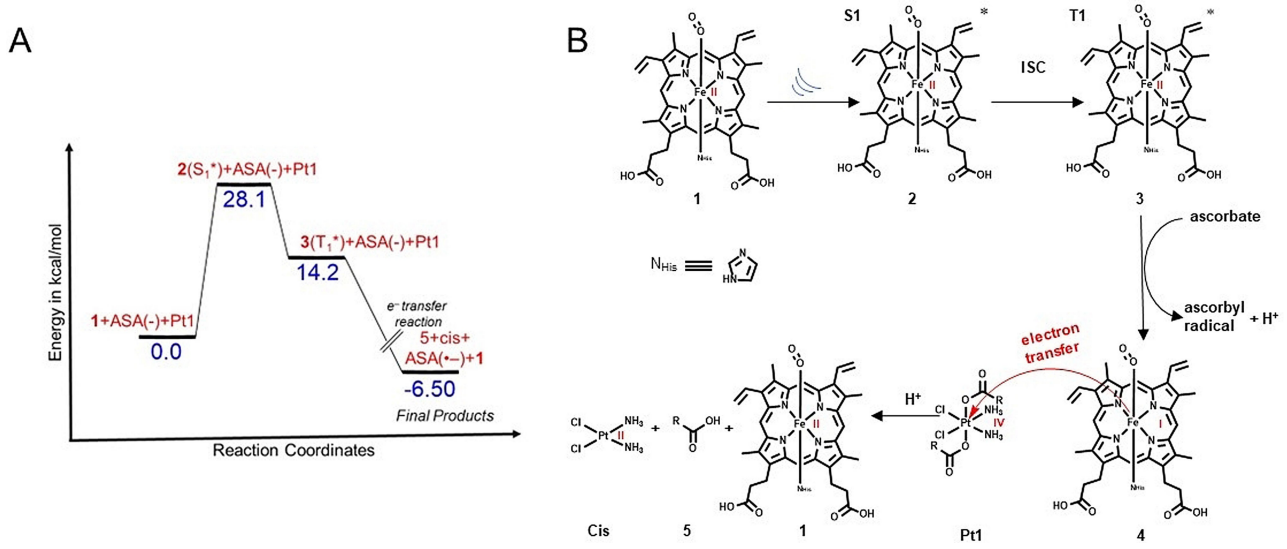


***Figure 1.*** Proposed mechanism of the reduction of the $Pt^{IV}$ prodrug **Pt1** with the sonosensitizer using DFT calculations. (A) Energy profile diagram of the reduction, indicative that the reaction is thermodynamically favored. (B) Proposed reduction mechanism.

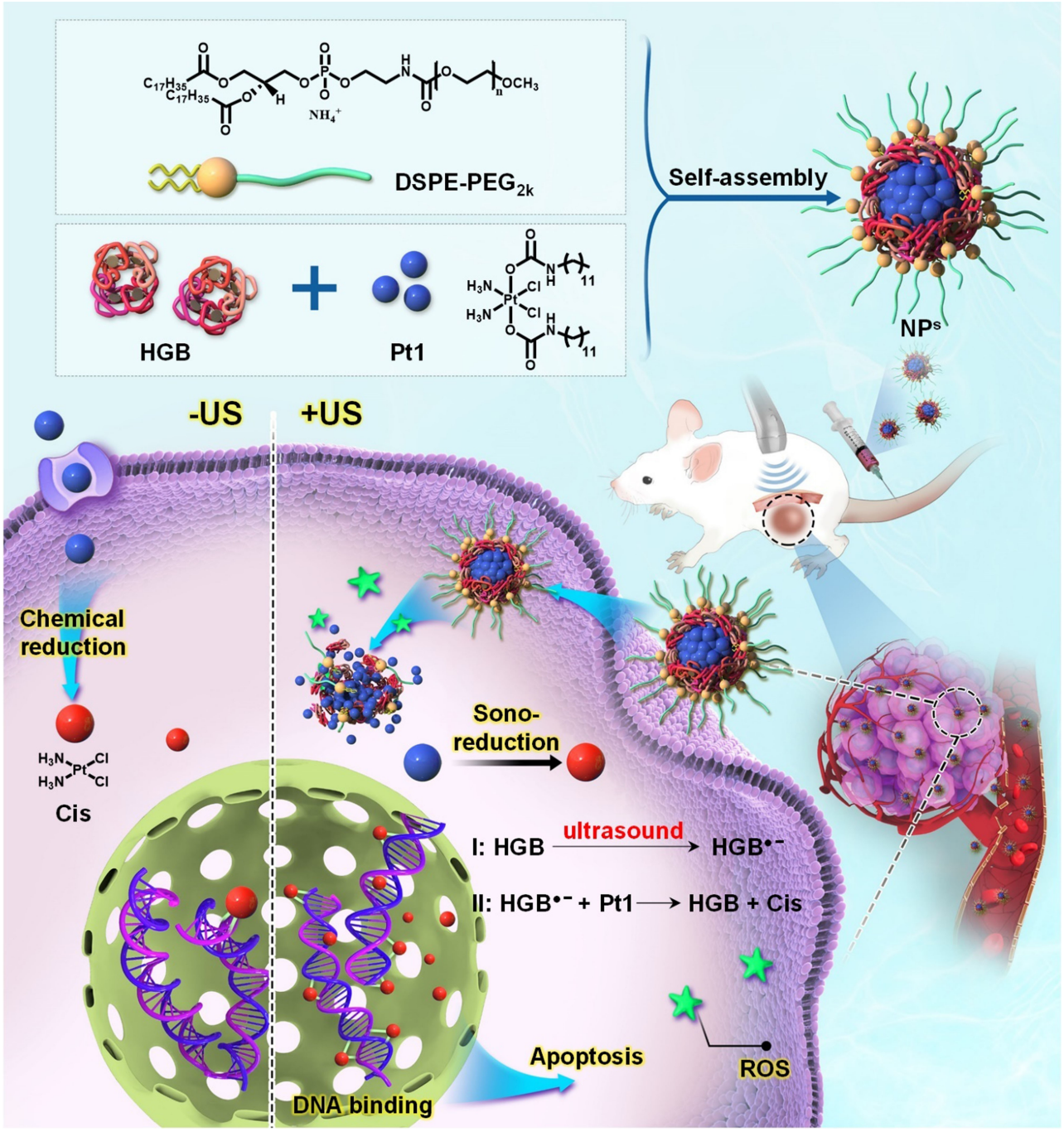


***Scheme 1.*** Illustration of the mechanism of action of **NP$^s$** for tumor-targeted, ultrasound-triggered anticancer therapy. Self-assembly of the sonosensitizer and drug carrier **hemoglobin** (**HGB**) with a hydrophobic Pt$^{IV}$ prodrug (**Pt1**) into nanoparticles (**NP$^s$**). The **NP$^s$** selectively accumulated at the tumor site upon injection into the bloodstream of a tumor-bearing mouse model. Upon exposure to ultrasound radiation, the Pt$^{IV}$ prodrug inside of the **NP$^s$** was rapidly reduced to cisplatin, causing the generation of ROS, DNA damage, and ultimately triggering cell death by apoptosis. US refers to ultrasound radiation.

the energy of this excited state could be directly but ineffectively transferred to the Pt$^{IV}$ prodrug, the theoretical calculations have indicated that the energy is more efficiently transferred to ascorbate as a mediator. The spin density plot of the excited triplet state of the Fe$^{II}$ sonosensitizer lies on the metal center, which can accept a π-electron from ascorbate, resulting in the formation of an unstable Fe$^{I}$ complex. The Fe$^{I}$ complex can further transfer an electron to the Pt$^{IV}$ complex, resulting in the desired reduction of the prodrug. The overall energetic balance indicated that this process is thermodynamically favored with an energetic difference of 6.5 kcal mol$^{-1}$ (frontier orbitals and spin density plots of the compounds: Table S1, coordinates of the compounds: Table S2, calculation of the energy differences

of the respective states: Table S3). It is important to mention that to date the molecular mechanism of sonosensitizers remains poorly understood. Previous studies have reported that when ultrasound radiation interacts with bulk liquid, it can create a unique phenomenon of cavitation. The implosion of these cavities can lead to extreme raises in temperature and pressure, which causes numerous chemical reactions, including the concentration of energy sufficient to generate light, known as sonoluminescence.[13] Within the following experiments, ultrasound radiation with a frequency of 1 MHz was used. DFT calculations indicate that this energy could be suitable for the excitation of **1**, presenting the feasibility of this approach.

Following this theoretical insight, the $Pt^{IV}$ complex **Pt1** was chemically synthesized. The identity of the compound was confirmed by nuclear magnetic resonance (NMR) and high-resolution electrospray ionization mass spectroscopy (HR-ESI-MS) and the purity was verified by high-performance liquid chromatography (HPLC) (Figure S3–S6). To investigate the potential reduction of the $Pt^{IV}$ prodrug into the analogous $Pt^{II}$ species upon release of the axial aliphatic chains, HPLC studies were performed (Figure 2A). As a facile model system, herein, the commercially available sonosensitizer **Hemin** was used. The incubation of **Pt1**, the co-incubation of **Pt1** with the sonosensitizer **Hemin**, or the exposure of **Pt1** to ultrasound radiation (1.5 W cm$^{-2}$, 10 min, Photograph of the experimental setup of the sonication of the solution: Figure S7) and incubation at 37 °C for 24 h resulted in a negligible amount of prodrug reduction (Figure 2B, Figure S8–S10). Contrary, the co-incubation of **Pt1** with the sonosensitizer **Hemin** as well as exposure to ultrasound radiation resulted in the reduction of the metal center and therefore activation of the prodrug. The reduction of **Pt1** was found to be approximately linear correlating with the prolongation of the radiation time as well as enhancement of the radiation power density (Figure 2C, Figure S11–S13), indicative that the release could be precisely controlled through external stimuli. Upon exposure of the solution to a radiation power density of 1.5 W cm$^{-2}$ for 10 min, approximately 31 % of the metal complex was found in its reduced form. Overall, these findings indicate that the prodrug **Pt1** is highly inert under

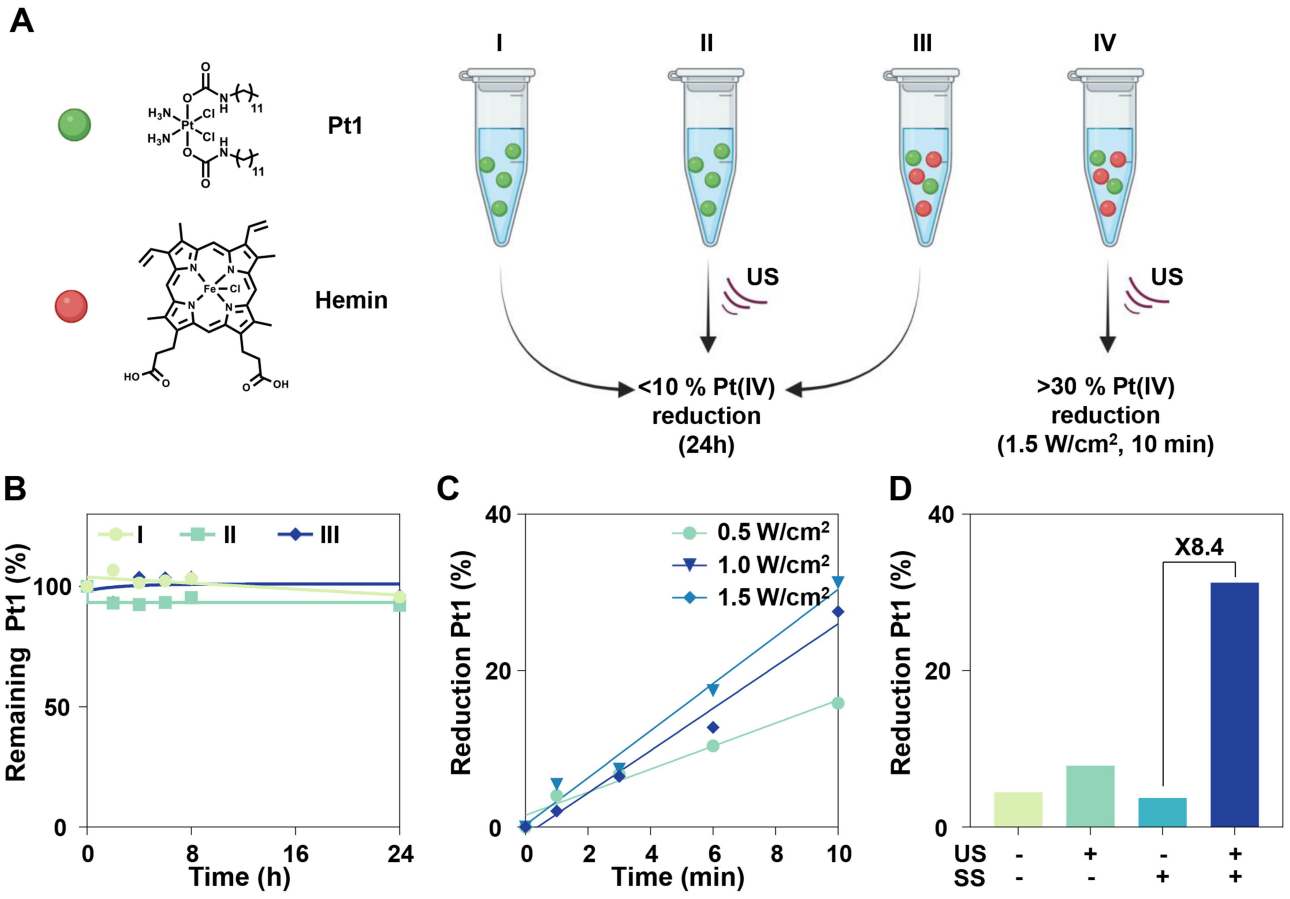


***Figure 2.*** Reduction of **Pt1** in the presence of a sonosensitizer **Hemin** and exposure to ultrasound radiation. (A) *Left:* Chemical structures of **Pt1** and **Hemin**. *Right:* Evaluation of the prodrug release under various conditions: (I) Incubation of **Pt1** at 37 °C for 24 h, (II) Incubation of **Pt1** at 37 °C for 24 h after exposure to ultrasound radiation (1.5 W cm$^{-2}$, 10 min), (III) Incubation of **Pt1** and **Hemin** at 37 °C for 24 h, (IV) Incubation of **Pt1** and **Hemin** and exposure to ultrasound radiation (1.5 W cm$^{-2}$, 10 min). (B) Time-dependent reduction of **Pt1** under conditions I–III. (C) Time-dependent reduction of **Pt1** under conditions IV upon variation of the radiation power density. (D) Comparison of the reduction of **Pt1** under various conditions at 37 °C for 24 h and exposure to ultrasound radiation (1.5 W cm$^{-2}$,10 min). US refers to ultrasound radiation.

physiological non-reducing conditions but can quickly be reduced in the presence of a sonosensitizer upon exposure to ultrasound radiation (Figure 2D). To the best of our knowledge, this study reports on the first example of the reduction of a $Pt^{IV}$ complex with ultrasound radiation.

Encouraged by these promising findings and to further enhance the therapeutic potential, herein, a multimodal nanoparticle formulation (**NP$^s$**) for tumor-targeted ultrasound radiation-triggered cancer therapy was designed. The strategy is based on the 1) use of Hemoglobin (**HGB**), a biologically naturally occurring protein with the desired heme group as a sonosensitizer; notably, the oxidation state of the metal core and the ligand environment of **Hemin** and the heme groups in **HGB** are different which could result in a different efficiency to act as a sonosensitizer; 2) encapsulation of the therapeutic $Pt^{IV}$ complex **Pt1** in the lipophilic protein center and therefore in the proximity of the heme group; 3) high biocompatibility of the nanoparticles; and 4) selective tumor accumulation due to the enhanced permeability and retention (EPR) effect of the nanomaterial. The ability to deliver the therapeutic metal complex to the tumor tissue as well as the necessity of the activation of the compound by ultrasound radiation allows for dual treatment targeting as well as improved therapeutic drug efficiency.

**HGB**, **Pt1**, and DSPE-$PEG_{2k}$ were self-assembled into nanoparticles by nanoprecipitation. Following the preparation, the particle size was analyzed by dynamic light scattering (DLS) measurements. **NP$^s$** were found with a hydrodynamic diameter of 174 nm and a polydispersity index of 0.25, indicative that the nanoparticles were well dispersed (Figure 3A). Transmission electron microscopy (TEM) measurements confirmed the particle size. The microscopy images further showed that the nanoparticles exerted a homogeneous spherical morphology (Figure 3B). Using scanning transmission electron microscopy (STEM) coupled with energy dispersive X-ray spectroscopy (EDX), the incorporation of the $Pt^{IV}$ complex into the supramolecular protein was studied. The images showed that the energetic signatures of the elements C, N, O, and Pt were evenly distributed in the nanomaterial, suggestive of the successful encapsulation of the metal complex (Figure 3C). The nanoparticles were found with a zeta potential of −12.9 mV, indicative of a negatively charged surface. For further characterization of the nano-assembly, the absorption profile of the nanoparticles was assessed. The absorption spectrum of **NP$^s$** showed the characteristic absorption band at 406 nm of **HGB** (Figure S14), indicative of the successful loading of **HGB** without affecting the energetic states of the respective moiety. Using the characteristic absorption band, the **HGB** concentration in **NP$^s$** was determined to be approximately 290 μM. As each HGB molecule consists of four subunits with each one heme group, an approximate concentration of heme was calculated to be 1160 μM. Using atomic absorption spectroscopy,

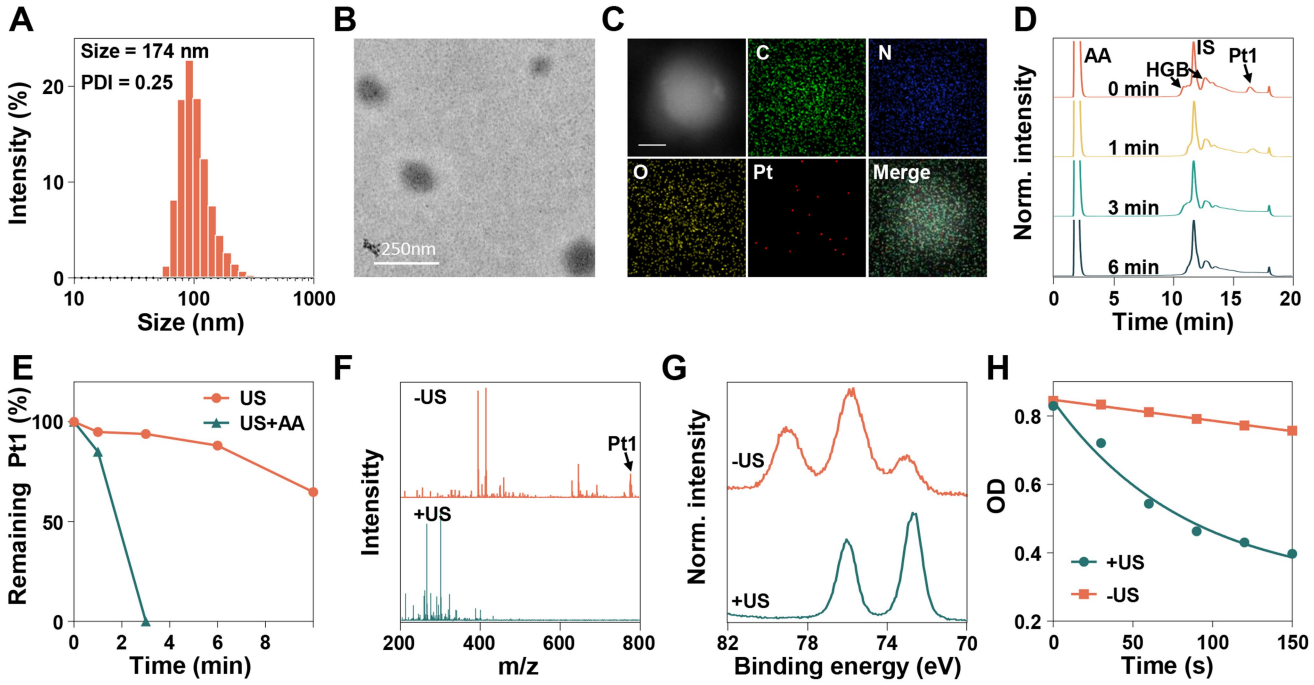


***Figure 3.*** Characterization of **NP$^s$** upon exposure to ultrasound radiation (1.5 W cm$^{-2}$, 10 min). (A) Dynamic light scattering measurements of **NP$^s$**. (B) Representative TEM images of **NP$^s$**. scale bar = 250 nm. (C) Representative high-angle annular dark-field scanning TEM (HAADF-STEM) images and the corresponding element mapping images of **NP$^s$**. Scale bar = 100 nm. (D) High-performance liquid chromatography chromatograms of the time-dependent incubation of **NP$^s$** to 5 mM ascorbic acid and exposure to ultrasound radiation. AA refers to ascorbic acid and IS refers to the internal standard triphenylphosphine oxide. (E) Time-dependent prodrug reduction from (D). (F) Electrospray ionization mass spectrum of **NP$^s$** in the dark or upon exposure to ultrasound radiation. (G) X-ray photoelectron spectrum of **NP$^s$** in the dark or upon exposure to ultrasound radiation. (H) Time-dependent monitoring of the characteristic absorption peak of the singlet oxygen probe 1,3-diphenylisobenzofuran upon incubation with **NP$^s$** in the dark or upon exposure to ultrasound radiation.

the concentration of Pt inside of **NP$^s$** was determined to be approximately 618 μM. This corresponds to an approximate ratio of 1:2 for **HGB**:**Pt1** and 2:1 for **heme**:**Pt1**.

The stability of the nanoparticles represents a crucial property for any medicinal application. Capitalizing on this, the stability in an aqueous solution for a period of 7 days was studied. Promisingly, no significant changes in the size or polydispersity of the nanoparticles were observed (Figure S15), indicative of the high stability under physiological conditions.

To study whether the formulation into nanoparticles has influenced the desired sono-reduction properties, the reduction of the $Pt^{IV}$ complex into the $Pt^{II}$ analogous species upon exposure to ultrasound radiation was studied by HPLC analysis. The results showed that 35 % of **Pt1** was reduced upon exposure to ultrasound radiation (1.5 W cm$^{-2}$) for 10 min. The amount of reduced species continuously increased with the prolongation of sonication time (Figure S16). Previous studies have indicated that $Pt^{IV}$ complexes could be reduced by ascorbic acid which is present in high concentrations in cancerous cells.[14] Capitalizing on this, the possible prodrug reduction in **NP$^s$** in the presence of ascorbic acid (5 mM) was studied. Upon incubation with ascorbic acid in water at 37 °C for 24 h in the dark, approximately 32 % of the metal complex was found to be reduced (Figure S17), indicative that the prodrug could be activated by intracellular reducing agents. Capitalizing on this, the reduction of the prodrug was studied by a dual prodrug activation mechanism through incubation with ascorbic acid (5 mM) as well as exposure to ultrasonic radiation (1.5 W cm$^{-2}$). Strikingly, within 3 min the $Pt^{IV}$ complex was fully converted into the analogous $Pt^{II}$ species (Figure 3D–3E), indicative of a stronger prodrug activation than the summation of the two triggers. For an experimental insight into the mechanism involved in the reduction of the prodrug, the magnetic susceptibility of **NP$^s$** was measured. The magnetic hysteresis loop indicated that the spin state of the $Fe^{II}$ center is S = 0 (Figure S18), indicative of the hexacoordinated oxy form.[15] These findings are in agreement with the proposed theoretical model (Figure 1). The reduction of the negatively charged $Pt^{IV}$ nanoparticles **NP$^s$** with the negatively charged ascorbate is counterintuitive. Previous studies have demonstrated that sonosensitizers and their corresponding nanoformulations that could not cross or enter specific biological systems were able to penetrate these upon exposure to ultrasound radiation. The authors have indicated that the modification of the biological properties was mediated through the inclusion into cavities that were generated upon exposure to ultrasound radiation.[16] Analogously, herein, the inclusion of **NP$^s$** and ascorbate into cavities with extreme temperature and pressure in which the reduction can take place is hypothesized. The prodrug reduction was further verified by electrospray ionization mass spectrometry (ESI-MS). While the mass spectrum of **NP$^s$** upon incubation in water at 37 °C for 24 h only showed the intact $Pt^{IV}$ prodrug ($m/z$ = 778 Da), upon exposure to ultrasound radiation a strongly reduced intensity of the $Pt^{IV}$ prodrug and the appearance of the $Pt^{II}$ product cisplatin ($m/z$ = 299 Da) was observed (Figure 3F). Complementary, the reduction of the metal center was monitored by X-ray photoelectron spectroscopy (XPS). The nanoparticles **NP$^s$** were found with the typical Pt4f binding energies at 79.1 and 75.7 eV which are associated with the +4 Pt oxidation state. Upon exposure to ultrasound radiation, these bands disappeared and peaks at 76.0 and 72.7 eV appeared which are associated with the +2 Pt oxidation state (Figure 3G). Combined these results indicate that the $Pt^{IV}$ complex inside of **NP$^s$** can be reduced into the analogous $Pt^{II}$ species upon exposure to ultrasound radiation.

The ability of **NP$^s$** to produce singlet oxygen ($^1O_2$) upon exposure to ultrasound radiation was investigated using the specific $^1O_2$ scavenger 1,3-diphenylisobenzofuran (DPBF). In the presence of $^1O_2$, 1,3-diphenylisobenzofuran can undergo a ring-opening reaction, resulting in a decrease of absorption at 410 nm. While no changes were observed upon co-incubation of DPBF with **NP$^s$**, a strong decrease of absorption at 410 nm was observed upon exposure of the solution to ultrasound radiation (1.5 W cm$^{-2}$, Figure 3H). Further analysis revealed that the decomposition rate constant of DPBF was 0.0051 s$^{-1}$. These results indicate that the heme in **HGB** can absorb energy of the ultrasound radiation upon excitation to an excited singlet state ($S^1$). Through an intersystem crossing process, an excited triplet state ($T^1$) is populated which can transfer its energy to molecular oxygen ($^3O_2$) upon formation of $^1O_2$.

As a prerequisite for the anticancer effect, the therapeutic agent needs to be internalized into the cancerous cells. To investigate the internalization of the nanomaterial, the **NP$^s$** were labeled with the fluorescent dye Cy5.5 to form **NP$^s$@Cy5.5** and the cellular uptake of **NP$^s$@Cy5.5** into mouse colon carcinoma (CT26) cells was studied by flow cytometry (Figure 4A, Figure S19). Complementary, the internalization was also investigated by confocal laser scanning microscopy (Figure S20). Upon prolongation of the incubation time, an increasing amount of nanoparticles was found inside the cancer cells. Using graphite furnace atomic absorption spectrometry (GF-AAS), the cellular uptake of Pt was quantified (Figure 4B). The results showed that the amount of Pt inside the cancer cells increased by 3.1 times upon prolongation of the incubation time from 1 h to 7 h. These findings indicate that the nanoparticles could be efficiently taken up into the cancer cells.

The ability of the nanoparticles to generate reactive oxygen species inside cancer cells was investigated by confocal laser scanning microscopy and flow cytometry using the probe 2,7-dichlorodihydrofluorescein diacetate. While this probe is non-fluorescent under non-oxidizing physiological conditions, in the presence of ROS the probe can be oxidized to the highly fluorescent 2,7-dichlorodihydrofluorescein. The treatment of the cancer cells with **Pt1** or **NP$^s$** in the dark showed only negligible amount of fluorescence. Contrary, strong green emission of the probe was monitored upon incubation of the cancer cells with **NP$^s$** and exposure to ultrasound radiation (Photograph of the experimental setup of the sonication of the cells: Figure S21, quantification by flow cytometry: Figure 4C and Figure S22, micro-

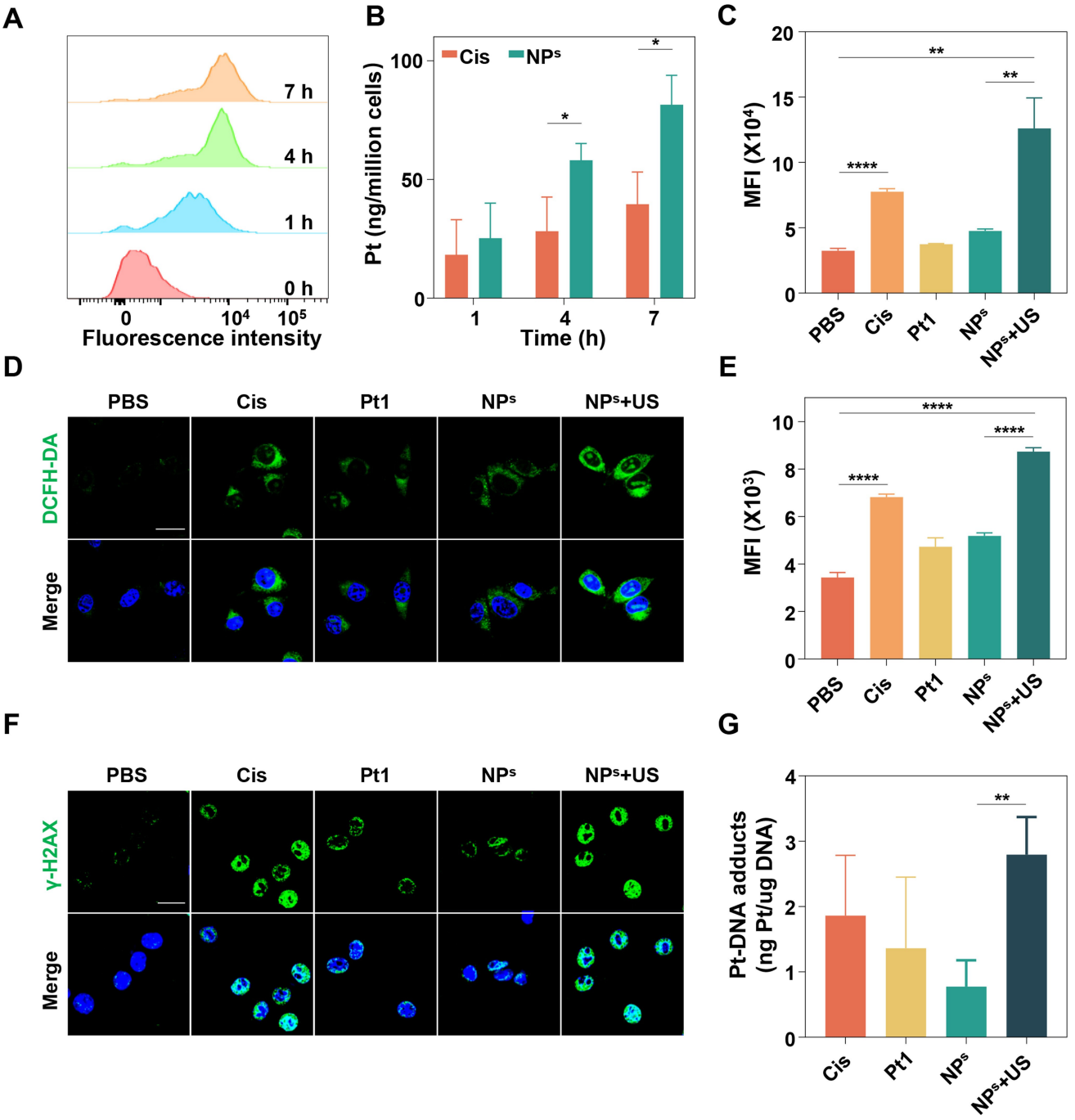


***Figure 4.*** Uptake, ROS generation, and DNA damage of CT26 cancer cells upon various treatments. (A) Flow cytometry plots of the cellular uptake of **NP$^s$@Cy5.5** over various time intervals. (B) Quantification of the cellular uptake of **NP$^s$** over various time intervals by GF-AAS. (C) Quantification of the ROS generation upon various treatments by flow cytometry. (D) Confocal laser scanning microscopy images of the ROS generation upon various treatments. Scale bar = 20 μm. (E) Quantification of the level of the DNA damage marker γ-H2AX upon various treatments by flow cytometry. (F) Confocal laser scanning microscopy images upon staining of γ-H2AX in CT26 cells upon various treatments. Scale bar = 20 μm. (G) Quantification of the level of Pt-DNA adducts upon various treatments by inductively coupled plasma mass spectrometry. US refers to ultrasound radiation. $n = 3$. Data are presented as mean ± standard deviation. Statistic significances between every two groups were calculated by one-way ANOVA test. *$p < 0.05$, **$p < 0.01$, ***$p < 0.001$, ****$p < 0.0001$.

scopy images: Figure 4D). These results indicate that the NP$^s$ could generate ROS in cancerous cells.

As the primary mechanism of action, Pt complexes are generally believed to bind to the DNA bases, causing cross-linking of the DNA, DNA damage, and ultimately cell death.[17] To investigate whether **NP$^s$** are able to therapeutically intervene with such a mechanism, the levels of the DNA damage marker γ-H2AX upon treatment were studied

by flow cytometry (Figure 4E, Figure S23). The quantification of the γ-H2AX levels suggested that the treatment with **NP$^s$** upon exposure to ultrasound radiation significantly upregulated the expression of γ-H2AX in the cancer cells. Complementary, the activation of γ-H2AX was assessed by an immunofluorescence staining study (Figure 4F). While only minimal γ-H2AX levels upon treatment with **Pt1** or **NP$^s$** in the dark were observed, significantly higher expression levels were monitored upon treatment with **Pt1** or **NP$^s$** upon exposure to ultrasound radiation (Figure 4F), indicative of severe DNA damage. Complementary, the amount of Pt-DNA adducts upon treatment was assessed by inductively coupled plasma mass spectrometry (ICP-MS). The results showed significantly higher levels of Pt-DNA adducts by treatment with **NP$^s$** upon exposure to ultrasound radiation than upon treatment with **Pt1** or **NP$^s$** in the dark (Figure 4G). Overall, these findings demonstrate that exposure to ultrasound radiation can trigger the reduction of $Pt^{IV}$ to $Pt^{II}$, resulting in an enhanced amount of Pt-DNA cross-links and DNA damage.

The therapeutic efficiency of the nanoparticles was assessed against mouse colon carcinoma (CT26), human hepatocellular carcinoma (BEL7404), and cisplatin-resistant human hepatocellular carcinoma (BEL7404DDP) cells using a cell counting kit-8 (CCK-8) assay. **Pt1** and **NP$^s$** were found to be poorly cytotoxic towards all tested cancer cell lines. In contrast, the treatment with **NP$^s$** upon exposure to ultrasound radiation caused a cytotoxic effect with half maximum inhibitory concentrations ($IC_{50}$) in the low micromolar range ($IC_{50,CT26} = 18 \pm 1$ μM, $IC_{50,BEL7404} = 16 \pm 1$ μM, $IC_{50,BEL7404DDP} = 24 \pm 2$ μM). The cytotoxic effect of **NP$^s$** was found to be in a similar range as for cisplatin (drug-response curves against CT26: Figure 5A, BEL7404: Figure 5B, BEL4704DDP: Figure 5C), indicative that **NP$^s$** are not able to overcome the cisplatin drug resistance of the cancer cells. To investigate whether other naturally occurring proteins or components inside the cancer cells are able to facilitate the reduction and therefore trigger a therapeutic cytotoxic effect, the cell viability of BEL7404DDP cells upon treatment with **Pt1**, **Pt1** upon exposure to ultrasound radiation, polymeric DSPE nanoparticles containing **Pt1** upon exposure to ultrasound radiation, **NP$^s$** in the dark, and **NP$^s$** upon exposure to ultrasound radiation were compared. The results showed that the treatment with **Pt1** in the dark did not cause a change in cell viability, indicative that the reduction is not or only poorly facilitated by intracellular reducing agents. The treatment with **Pt1** or polymeric nanoparticles containing **Pt1** upon exposure to ultrasound radiation did not cause a significant cytotoxic effect, highlighting the importance of the sonosensitizer **HGB** as well as suggesting that the reduction cannot be efficiently induced by other naturally occurring proteins. While the treatment with **NP$^s$** in the dark did not trigger a therapeutic effect, a cytotoxic effect in the low micromolar range was observed upon the treatment with **NP$^s$** upon exposure to ultrasound radiation. These findings clearly highlight the necessity of **HGB** as a sonosensitizer for the therapeutic effect.

For a deeper understanding of the cell death mechanism, the percentage of cancer cells in an apoptotic stage upon treatment was determined by flow cytometry using Annexin V-FITC and propidium iodide double staining. While the treatment of CT26 cells with **Pt1** and **NP$^s$** showed only a small number of apoptotic cells, the incubation of the cancer cells with **NP$^s$** upon exposure to ultrasound radiation resulted in a significantly higher percentage of cells in an apoptotic stage (flow cytometry plot: Figure 5D, quantification of apoptotic cells: Figure 5E). To evaluate the antiproliferative effect, a colony formation assay was performed. The treatment with **NP$^s$** upon exposure to ultrasound radiation showed a strongly reduced number of colonies, indicative of its possible long-term anticancer effect (Figure 5F). Combined these findings highlight that **NP$^s$** are able to efficiently trigger cancer cell death.

Based on the promising effects of the nanoparticles against two-dimensional monolayer cancer cells, the therapeutic properties against three-dimensional multicellular tumor spheroids were studied. Multicellular tumor spheroids are a tissue culture model that more realistically describes the pharmacological properties of solid tumors including proliferation gradients, oxygen gradients, and intercellular architectures.[18] The therapeutic effect against CT26 multicellular tumor spheroids was investigated by fluorescence microscopy using live and dead staining. While the multicellular tumor spheroids treated with **Pt1** and **NP$^s$** majorly consisted of living cancer cells, most cells in the multicellular tumor spheroids treated with **NP$^s$** upon exposure to ultrasound radiation were dead (Figure 5G).

Encouraged by the promising properties inside the cellular model, the biological properties of the nanoparticles were further studied in a CT26 tumor-bearing mouse model (Figure 6A). To investigate the biodistribution inside the mouse model, **NP$^s$@Cy5.5** was intravenously injected and the fluorescence signal was monitored (Figure 6B). After 36 h, the maximal fluorescence intensity at the tumor site was observed (Figure 6C). After 72 h, the mice were sacrificed and the accumulation of the nanoparticles in the major organs was analyzed by fluorescence imaging (Figure 6B). Impressively, the vast majority of the injected doses accumulated at the tumor site (Figure 6D). These findings highlight the high potential of the nanoparticles for tumor-targeted therapy.

To study the therapeutic efficiency, CT26 tumor-bearing mice were intravenously injected with phosphate-buffered saline (PBS), cisplatin, or **NP$^s$** (1.5 mg kg$^{-1}$) on days 0 and 3. The animals which were exposed to ultrasound radiation, were treated for 5 min with a portable ultrasonic apparatus (DJO Chattanooga 2776, USA) on days 1 and 4. To highlight the ability of this medicinal technique for the treatment of very large or deep-seated tumors, a specific treatment group was set up in which a 2 cm wide piece of chicken breast was placed as a barrier before the tumor (Photograph of the experimental setup of the sonication of the mouse model: Figure S24). The tumor volume and body weight of the mice were recorded every two days. The tumor volume of the mice treated with phosphate-buffered saline or purely with the ultrasound radiation grew asymptotically in the same manner, indicative that these treatments do not influence tumor growth. The tumors of the mice treated

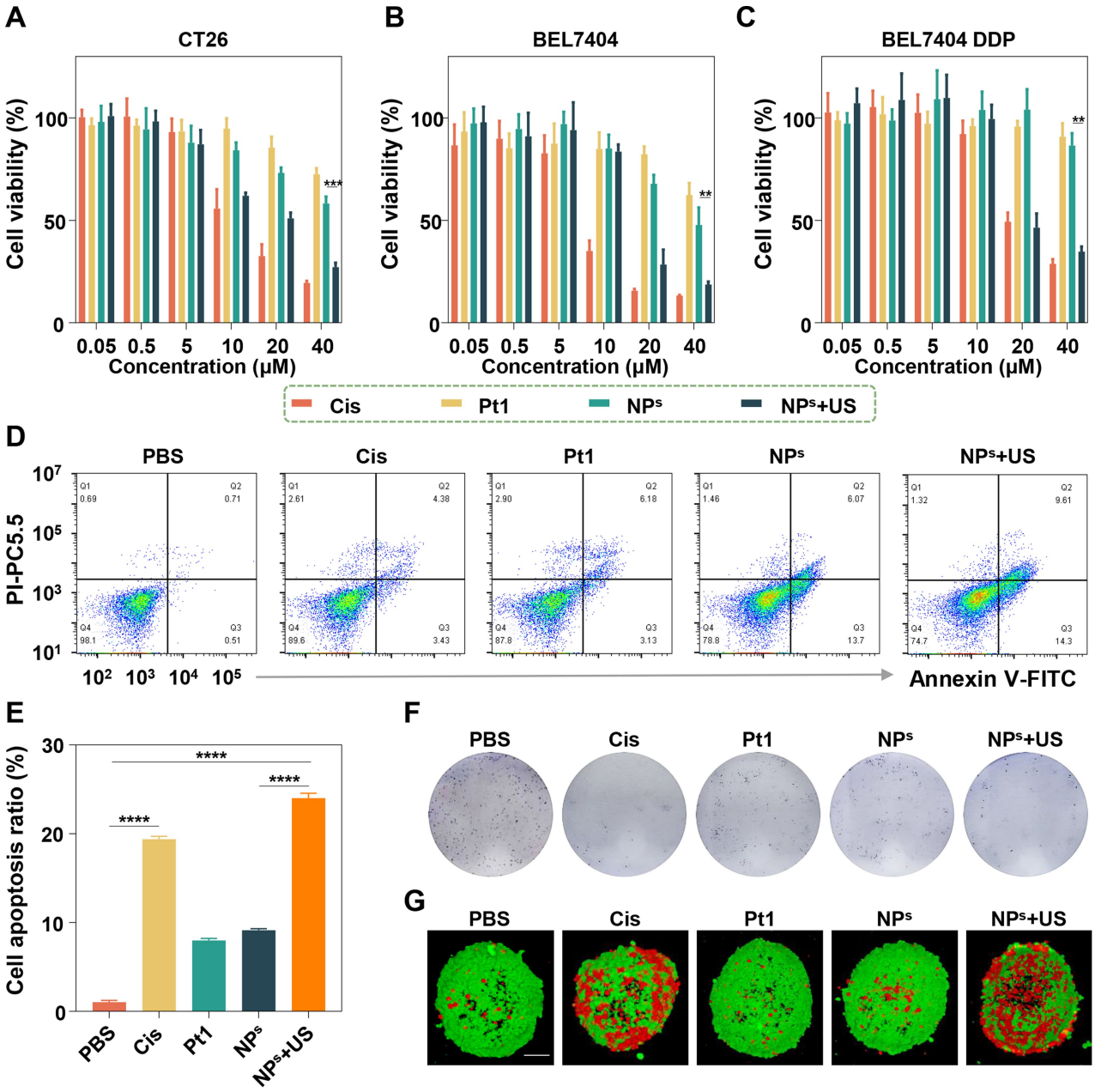


***Figure 5.*** Cytotoxicity upon treatment of cancer cells or multicellular tumor spheroids with **NP$^s$+US**. (A–C) Drug response curves upon various treatments. (D) Flow cytometry plots of apoptotic cells upon various treatments. (E) Quantification of apoptotic cells from (D). (F) Colony formation assay upon various treatments. (G) Confocal laser scanning microscopy images of CT26 multicellular tumor spheroids with a cell live/dead staining upon various treatments. Scale bar = 100 μm. US refers to ultrasound radiation. $n = 3$. Data are presented as mean ± standard deviation. Statistic significances between every two groups were calculated by one-way ANOVA test. *$p < 0.05$, **$p < 0.01$, ***$p < 0.001$, ****$p < 0.0001$.

with **NP$^s$** in the dark showed a slight tumor growth inhibition effect due to prodrug activation by the cancer microenvironment. In contrast, the tumors treated with **NP$^s$** and exposed to ultrasound radiation were nearly fully eradicated. Strikingly, even the tumors that were covered with an additional chicken breast barrier were nearly fully eradicated. These findings emphasize that the activation of the prodrug through ultrasound radiation could be useful for the treatment of deep-seated or very large tumors (Figure 6E). Importantly, the mice behaved normally throughout the treatment period without significant loss of weight (Figure 6F), indicative of the high biocompatibility of the treatment. After the treatment period (14 days), the animal models were sacrificed. A visual inspection of the tumors clearly shows the strong therapeutic efficacy of the nanoparticles. Three of the phosphate-buffered saline and three of the purely ultrasound radiation-treated mice were sacrificed prematurely because the tumors had reached the

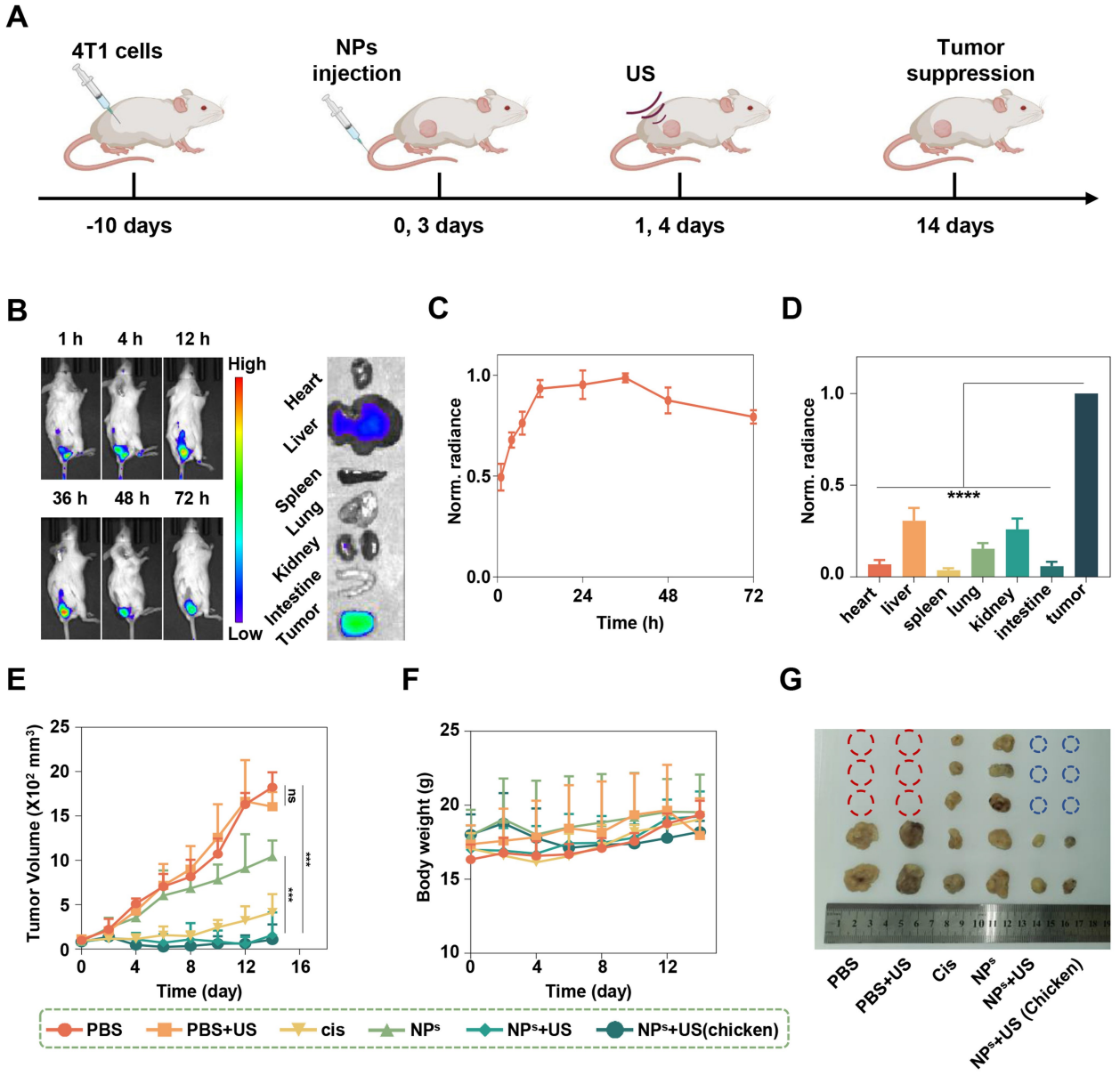


***Figure 6.*** Biodistribution and tumor growth inhibition effect in a CT26 tumor-bearing mouse model upon intravenous injection of **NP$^s$** (1.5 mg Pt/kg body weight) and exposure to ultrasound radiation (1.5 W cm$^{-2}$, 5 min). (A) Schematic illustration of the treatment schedule. (B) *Left*: In vivo distribution of **NP$^s$@Cy5.5** determined by fluorescence bio-imaging. *Right*: Ex vivo imaging of tumors and major organs 72 h after administration of **NP$^s$@Cy5.5**. (C) Time-dependent accumulation of **NP$^s$@Cy5.5** at the tumor site. (D) Biodistribution 72 h after administration of **NP$^s$@Cy5.5**. (E) Tumor growth inhibition curves upon various treatments. (F) Changes of body weight of mice upon various treatments. (G) Representative photograph of the tumors 14 days after the treatment. The red circle represents premature sacrifice of the mice and the blue circle represents complete eradication of the tumor. (H) H&E and TUNEL staining of the tumor tissues upon various treatments. Scale bar = 100 μm. US refers to ultrasound radiation. $n = 3$–5. Data are presented as mean ± standard deviation. Statistic significances between every two groups were calculated by one-way ANOVA test. *$p < 0.05$, **$p < 0.01$, ***$p < 0.001$, ****$p < 0.0001$.

ethically acceptable maximum. In contrast, the tumors which were treated with **NP$^s$** and exposed to ultrasound radiation were fully eradicated (Figure 6G). For a deeper understanding of the therapeutic effect, the tumorous tissues were histologically analyzed by hematoxylin and eosin (H&E) staining and terminal deoxynucleotidyl transferase-mediated dUTP-biotin nick end labeling (TUNEL). The microscopy images of the tumorous tissues treated with **NP$^s$** and exposed to ultrasound radiation showed nuclear fragmentation, nucleolysis of the tumor cells, as well as DNA damage (Figure 6H). Overall, these findings highlight the strong therapeutic potential of **NP$^s$** as an ultrasound radiation-activated prodrug for tumor-targeted cancer therapy.

## Conclusion

In summary, this study reports on the first example of the activation of $Pt^{IV}$ prodrug nanoparticles upon exposure to ultrasound radiation for deep tissue penetrating anticancer therapy. While remaining stable under physiological conditions, the $Pt^{IV}$ complex was reduced in the presence of a sonosensitizer and exposure to ultrasound radiation into the respective $Pt^{II}$ species. To improve the water solubility and provide cancer selectivity, the metal complex was encapsulated with the biocompatible sonosensitizer hemoglobin into nanoparticles. Studies in mouse colon carcinoma cells revealed that the nanoparticles rapidly dissociate in cancerous cells which were exposed to ultrasound radiation, triggering cell death by apoptosis. The biological properties were further tested in colon carcinoma-bearing mouse models. Encouragingly, the nanoparticles were found to selectively accumulate inside the tumor upon intravenous injection. To highlight the ability of this medicinal technique for the treatment of very large or deep-seated tumors, the tumor tissue was covered with an additional 2 cm wide piece of chicken breast as a barrier. Upon exposure of the tumor to ultrasound radiation, the tumors were completely eradicated in nearly all mouse models. These findings highlight the high potential of this form of treatment for very large or deep-seated tumors and are expected to open new avenues for the treatment of cancer.

## Author Contributions

DFT calculations were performed by T.S. Chemical, photophysical, and biological experiments were performed by G. L., D. T., H. Z., and M. C. The work was supervised by J. K. and H. X. All authors have given approval to the final version of this paper.

## Acknowledgements

This work is supported by the National Key Research & Development Program (2022YFC2603900), Central Government Guided Local Science and Technology Development Fund (Hebei) (216Z2601G), and the National Natural Science Foundation of China (22175189). All animal experiments were conducted in accordance with the guidelines of the Ethics Committee of Peking University (project number: LA2021316). S.B. thanks IIT BHU supercomputing facilities and SERB (SRG/2022/000030), the Government of India for funding. J.K. gratefully acknowledges the financial support with a Liebig fellowship from the Chemical Industry Fund of the German Chemical Industry Association. The schematic illustrations in Scheme 1 and Figure 6 are created with BioRender.com. Open Access funding enabled and organized by Projekt DEAL.

## Conflict of Interest

The authors declare no conflict of interest.

## Data Availability Statement

The data that support the findings of this study are available in the supplementary material of this article.

**Keywords:** Bioinorganic Chemistry · Medicinal Inorganic Chemistry · Metals in Medicine · Platinum · Ultrasound Radiation

[1] a) L. Kelland, *Nat. Rev. Cancer* **2007**, *7*, 573–584; b) G. Kim, H. L. Tan, R. Sundar, B. Lieske, C. E. Chee, J. Ho, A. Shabbir, M. V. Babak, W. H. Ang, B. C. Goh, W. P. Yong, L. Wang, J. B. Y. So, *Clin. Cancer Res.* **2021**, *27*, 1875–1881.

[2] a) E. Armstrong-Gordon, D. Gnjidic, A. J. McLachlan, B. Hosseini, A. Grant, P. J. Beale, N. J. Wheate, *J. Cancer Res. Clin. Oncol.* **2018**, *144*, 1561–1568; b) J. Karges, R. W. Stokes, S. M. Cohen, *Trends Chem.* **2021**, *3*, 523–534.

[3] a) D. Wang, S. J. Lippard, *Nat. Rev. Drug Discovery* **2005**, *4*, 307–320; b) A. Eskandari, A. Kundu, S. Ghosh, K. Suntharalingam, *Angew. Chem. Int. Ed.* **2019**, *58*, 12059–12064; c) M. J. R. Tham, M. V. Babak, W. H. Ang, *Angew. Chem. Int. Ed.* **2020**, *59*, 19070–19078; d) Y. Guo, S. Jin, H. Yuan, T. Yang, K. Wang, Z. Guo, X. Wang, *J. Med. Chem.* **2022**, *65*, 520–530.

[4] a) T. C. Johnstone, K. Suntharalingam, S. J. Lippard, *Chem. Rev.* **2016**, *116*, 3436–3486; b) X. Wang, X. Wang, S. Jin, N. Muhammad, Z. Guo, *Chem. Rev.* **2019**, *119*, 1138–1192; c) M. V. Babak, Y. Zhi, B. Czarny, T. B. Toh, L. Hooi, E. K.-H. Chow, W. H. Ang, D. Gibson, G. Pastorin, *Angew. Chem. Int. Ed.* **2019**, *58*, 8109–8114; d) Y.-R. Zheng, K. Suntharalingam, T. C. Johnstone, H. Yoo, W. Lin, J. G. Brooks, S. J. Lippard, *J. Am. Chem. Soc.* **2014**, *136*, 8790–8798; e) J. Karges, T. Yempala, M. Tharaud, D. Gibson, G. Gasser, *Angew. Chem. Int. Ed.* **2020**, *59*, 7069–7075; f) C. Schmidt, T. Babu, H. Kostrhunova, A. Timm, U. Basu, I. Ott, V. Gandin, V. Brabec, D. Gibson, *J. Med. Chem.* **2021**, *64*, 11364–11378; g) X. Wang, X. Wang, Z. Guo, *Acc. Chem. Res.* **2015**, *48*, 2622–2631.

[5] a) W. Wang, J. Cai, J. Wen, X. Li, Y. Yu, L. Zhang, Q. Han, Z. Wei, Y. Ma, F. Ying, X. Xu, W. Li, Q. Yang, S. Sun, X. He, L. Cai, H. Xiao, Z. Wang, *Nano Today* **2022**, *44*, 101459; b) X. Gao, G. Lei, B. Wang, Z. Deng, J. Karges, H. Xiao, D. Tan, *Adv. Sci.* **2022**, *10*, 2205241; c) L. Cao, H. Tian, M. Fang, Z. Xu, D. Tang, J. Chen, J. Yin, H. Xiao, K. Shang, H. Han, X. Li, *Biomaterials* **2022**, *290*, 121856; d) Y. Wang, Y. Jiang, D. Wei,

P. Singh, Y. Yu, T. Lee, L. Zhang, H. K. Mandl, A. S. Piotrowski-Daspit, X. Chen, F. Li, X. Li, Y. Cheng, A. Josowitz, F. Yang, Y. Zhao, F. Wang, Z. Zhao, A. Huttner, R. S. Bindra, H. Xiao, W. Mark Saltzman, *Nat. Biomed. Eng.* **2021**, *5*, 1048; e) D. Wei, Y. Yu, X. Zhang, Y. Wang, H. Chen, Y. Zhao, F. Wang, G. Rong, W. Wang, X. Kang, J. Cai, Z. Wang, J. Yin, M. Hanif, Y. Sun, G. Zha, L. Li, G. Nie, H. Xiao, *ACS Nano* **2020**, *14*, 16984–16996; f) J. J. Wilson, S. J. Lippard, *Inorg. Chem.* **2011**, *50*, 3103–3115.

[6] a) J. X. Ong, C. S. Q. Lim, H. V. Le, W. H. Ang, *Angew. Chem. Int. Ed.* **2019**, *58*, 164–167; b) S. Yuan, Y. Zhu, Y. Dai, Y. Wang, D. Jin, M. Liu, L. Tang, F. Arnesano, G. Natile, Y. Liu, *Angew. Chem. Int. Ed.* **2022**, *61*, e202114250; c) Z. Xu, Z. Wang, Z. Deng, G. Zhu, *Coord. Chem. Rev.* **2021**, *442*, 213991.

[7] a) Y. Min, J. Li, F. Liu, E. K. L. Yeow, B. Xing, *Angew. Chem. Int. Ed.* **2014**, *53*, 1012–1016; b) Z. Deng, N. Wang, Y. Liu, Z. Xu, Z. Wang, T.-C. Lau, G. Zhu, *J. Am. Chem. Soc.* **2020**, *142*, 7803–7812; c) N. J. Farrer, J. A. Woods, L. Salassa, Y. Zhao, K. S. Robinson, G. Clarkson, F. S. Mackay, P. J. Sadler, *Angew. Chem. Int. Ed.* **2010**, *49*, 8905–8908; d) E. M. Bolitho, C. Sanchez-Cano, H. Shi, P. D. Quinn, M. Harkiolaki, C. Imberti, P. J. Sadler, *J. Am. Chem. Soc.* **2021**, *143*, 20224–20240; e) J. Karges, *Angew. Chem. Int. Ed.* **2022**, *61*, e202112236; f) C. A. Wootton, C. Sanchez-Cano, A. F. Lopez-Clavijo, E. Shaili, M. P. Barrow, P. J. Sadler, P. B. O'Connor, *Chem. Sci.* **2018**, *9*, 2733–2739; g) E. Shaili, L. Salassa, J. A. Woods, G. Clarkson, P. J. Sadler, N. J. Farrer, *Chem. Sci.* **2019**, *10*, 8610–8617; h) Z. Huang, A. P. King, J. Lovett, B. Lai, J. J. Woods, H. H. Harris, J. J. Wilson, *Chem. Commun.* **2021**, *57*, 11189–11192.

[8] Z. Wang, N. Wang, S.-C. Cheng, K. Xu, Z. Deng, S. Chen, Z. Xu, K. Xie, M.-K. Tse, P. Shi, H. Hirao, C.-C. Ko, G. Zhu, *Chem* **2019**, *5*, 3151–3165.

[9] D. Wei, Y. Huang, B. Wang, L. Ma, J. Karges, H. Xiao, *Angew. Chem. Int. Ed.* **2022**, *61*, e202201486.

[10] a) B. C. Wilson, W. P. Jeeves, D. M. Lowe, *Photochem. Photobiol.* **1985**, *42*, 153–162; b) J. Karges, H. Chao, G. Gasser, *J. Biol. Inorg. Chem.* **2020**, *25*, 1035–1050; c) L. C.-C. Lee, K. K.-W. Lo, *J. Am. Chem. Soc.* **2022**, *144*, 14420–14440.

[11] a) J. Ouyang, Z. Tang, N. Farokhzad, N. Kong, N. Y. Kim, C. Feng, S. Blake, Y. Xiao, C. Liu, T. Xie, W. Tao, *Nano Today* **2020**, *35*, 100949; b) C. Errico, J. Pierre, S. Pezet, Y. Desailly, Z. Lenkei, O. Couture, M. Tanter, *Nature* **2015**, *527*, 499–502.

[12] a) X. Pang, C. Xu, Y. Jiang, Q. Xiao, A. W. Leung, *Pharmacol. Ther.* **2016**, *162*, 144–151; b) A. P. McHale, J. F. Callan, N. Nomikou, C. Fowley, B. Callan, in *Therapeutic Ultrasound, Vol. 880* (Eds.: J. M. Escoffre, A. Bouakaz), **2016**, pp. 429–450; c) A. Steinbrueck, J. Karges, *ChemBioChem* **2023**, *24*, e202300079.

[13] L. Pauling, C. D. Coryell, *Proc. Natl. Acad. Sci. USA* **1936**, *22*, 210–216.

[14] a) X. Lin, J. Song, X. Chen, H. Yang, *Angew. Chem. Int. Ed.* **2020**, *59*, 14212–14233; b) H. Shibaguchi, H. Tsuru, M. Kuroki, M. Kuroki, *Anticancer Res.* **2011**, *31*, 2425–2429.

[15] M. Sinisi, F. P. Intini, G. Natile, *Inorg. Chem.* **2012**, *51*, 9694–9704.

[16] a) H. Chen, S. Zhang, Q. Fang, H. He, J. Ren, D. Sun, J. Lai, A. Ma, Z. Chen, L. Liu, R. Liang, L. Cai, *ACS Nano* **2023**, *17*, 421–436; b) A. Dasgupta, M. Liu, T. Ojha, G. Storm, F. Kiessling, T. Lammers, *Drug Discovery Today Technol.* **2016**, *20*, 41–48; c) Z. Ma, C. Bourquard, Q. Gao, S. Jiang, T. De Iure-Grimmel, R. Huo, X. Li, Z. He, Z. Yang, G. Yang, Y. Wang, E. Lam, Z. Gao, O. Supponen, J. Li, *Science* **2022**, *377*, 751–755.

[17] a) J. J. Roberts, J. M. Pascoe, *Nature* **1972**, *235*, 282–284; b) S. Dasari, P. B. Tchounwou, *Eur. J. Pharmacol.* **2014**, *740*, 364–378.

[18] J. Karges, S. Kuang, Y. C. Ong, H. Chao, G. Gasser, *Chem. Eur. J.* **2021**, *27*, 362–370.

Manuscript received: January 20, 2023
Accepted manuscript online: March 24, 2023
Version of record online: April 19, 2023